Journal of Computational Applied Mechanics 2026, 57(3): 369-390

DOI: 10.22059/jcamech.2026.410638.1780

RESEARCH PAPER

CFD Simulation of the Aqueous Humour in Healthy or Glaucomatous Conditions

O. Anwar Bég [a], U.I. Usman [b], Tasveer A. Bég [c], M. M. Channakote [d], H. J. Leonard [a], Muhammad Mubashir Bhatti [e,f,*]

[a] *Multi-Physical Engineering Sciences Group, Mechanical Engineering Department, Corrosion and Coatings Lab, Room 3-08, SEE Building, University of Salford, Manchester, M54WT, UK*

[b] *Simulation Engineer, Shell Petroleum, London, UK*

[c] *Engineering Mechanics Research, Israfil House, Dickenson Rd., Manchester, M13, UK*

[d] *Department of Mathematics and Statistics, M. S. Ramaiah University of Applied Sciences, Bengaluru, Karnataka, 560054, India*

[e] *Department of Physics, College of Science, Korea University, 145 Anam-ro, Seongbuk-gu, Seoul 02841, Republic of Korea*

[f] *Material Science Innovation and Modelling (MaSIM) Research Focus Area, North-West University (Mafikeng Campus), Private Bag X2046, Mmabatho 2735, South Africa*

Abstract

This article presents a computational fluid dynamics (CFD) simulation of aqueous humour flow within the anterior chamber of the eye, comparing healthy and glaucomatous conditions. A simplified 2-dimensional cross-sectional geometry was developed using ANSYS Fluent 2024 R2 Design Modeller, with the trabecular meshwork represented as a porous medium, accounting for its role in flow resistance. Viscous resistances of 2.43 x 10^{13} m^{-2} and 6.5 x 10^{13} m^{-2} for healthy and glaucomatous cases respectively, were derived from literature and applied to simulate variations in the outflow. A mesh independence study was included. In the healthy model, the simulation peak intraocular pressure of 15.08 mmHg was consistent with normal physiological limits. In the glaucomatous case, intraocular pressure increased to 40.45 mmHg, representing a 168% rise, also agreeing with existing literature. The visualisation of flow fields revealed similar inlet velocity profiles but notable differences in pressure gradients, streamline curvature and vorticity distribution near the trabecular meshwork in the glaucomatous configuration. These numerical trends are within ±5% of existing literature results and confirm the validity of the study. The anterior chamber's fluid sensitivity is clearly highlighted in the results, confirming the role of CFD as a predictive tool for understanding ocular fluid mechanics and supporting diagnostic and surgical decision making in glaucoma management.

Keywords: Ocular fluid dynamics; aqueous humour; anterior chamber; glaucomatous conditions; trabecular meshwork; Darcy porous medium; intraocular pressure; streamline curvature.

1. Introduction

The human eye, a specialised organ for visual and spatial awareness, works as an optical system biologically designed to require precise fluid dynamics conditions for it to regulate intraocular pressure (IOP), support the

* Corresponding author. *E-mail address:* mmbhatti@korea.ac.kr

metabolism of the human body, and maintain structural integrity. The aqueous humour (AH), a clear fluid sited in the anterior chamber of the eye, is produced by the ciliary body, flowing through the pupil and leaving the eye through the trabecular meshwork (TM) and Schlemm's canal (SC). These two pathways are known as the conventional outflow pathway. Glaucoma has been observed to develop as a result of the disruption of the circulatory process in the outflow interface. Glaucoma is the leading cause of blindness worldwide, and according to the World Health Organisation (WHO), an estimated 76 million people are affected by glaucoma, with a projected increase to 112 million people by 2040. Glaucoma is characterised by decreasing efficiency of the optic nerve, caused by high IOP due to the impaired drainage of the AH fluid. Although there are two forms of glaucoma namely primary open-angle glaucoma (POAG) and primary angle-closure glaucoma (PACG), the latter is more commonly seen among Asian and African populations and presents a more difficult challenge to eyesight, as noted by Murgoitio-Esandi *et al.* [1]. Researching AH dynamics is essential to accurately diagnose and treat glaucoma, but is also necessary to develop surgical tools, pressure regulating devices (such as the Ahmed glaucoma valves), and drug delivery systems. Despite being one of the most significant organs of the human body, the eye remains vastly understudied in comparison to the other physiological systems. This is mostly due to the complexities in its anatomy and ethical considerations in experimental studies. The increasing global prevalence of glaucoma in society especially among the elderly highlights a global need for urgency in the development of diagnostic tools that can be accurate and non-invasive. In the field of ophthalmology, there is a strong commercial case for CFD applications, where companies are investing significantly in the development of ocular implants, contact lenses and surgical tools, using the results of high-precision simulations that significantly cut prototyping cost and design optimisation time. Horner and Missel [2] confirmed the viability of ANSYS Fluent as a reliable method for simulating drug delivery and thermal transport conditions in the eye, buttressing the point in favour computational fluid dynamics (CFD) models being used industrially for research purposes. Therefore, (CFD) modelling of the eye provides a viable platform for the advancement of scientific and clinical knowledge. Using CFD simulations visuals of intraocular fluid behaviour can be provided under different conditions, aiding clinicians in the early diagnosis and surgical treatment of glaucoma, as elaborated by Fitt and Gonzalez [3]. They developed one of the first analytical models for AH circulation in the anterior. chamber, focusing on corneal cooling caused by natural convection. They used the Boussinesq approximation to simulate laminar buoyancy-driven flow, showing the role of thermal gradients on the patterns of intraocular circulation. Their prediction of a clockwise vortex within the anterior chamber was confirmed by later numerical simulations. These contributions are foundational to thermal understanding of ocular fluid dynamics and flow drivers, including when there is absence of pressure differentials. Ocular fluid dynamics research has proven to be a very promising area of consideration for medical treatments; however, several difficulties persist that are important to explore. CFD models are mostly based on geometric simplifications and assumed material and fluid properties, which may not capture the many changes possible in human eyes anatomically and physiologically fully. For example, Issarti *et al.* [4] demonstrated the importance of anatomical structures like the lens and iris, by proving that an exclusion of these structures alters the pressure and velocity fields, introducing a limitation to the use of 2D models in real-life situations. They used COMSOL to apply ALE (Arbitrary Lagrangian-Eulerian) techniques in the modelling of deformation in ocular tissues under increasing IOP, focusing on the displacement of the iris and cornea. Their study proposes a direction for future research through the confirmation of the importance of mechanical responses under elevated IOP conditions described in their study. Studies conducted by Ethier *et al.* [5] and later Villamarin *et al.* [6] have noted the challenge in assigning realistic boundary conditions, due to a lack of experimental data on aqueous flow rates and outflow pressures at microscopic levels, making it challenging to validate the results of simulations without vivo measurements. They conducted a 3D simulation of the eye using ANSYS Fluent, highlighting the importance of curvature in the determination of streamline behaviours and stability of flow. Unlike the simplified 2D axisymmetric assumptions common in most ocular fluids research studies, the use of 3D geometry in their study allows closer analysis of spatial variations in flow parameters. Also, the vast majority of CFD models assume that the behaviour of the eyes fluids is steady-state, incompressible and Newtonian. This is a simplification that helps with the numerical calculations but sacrifices transient phenomena such as blinking-induced pulsatile flow, diurnal variations in AH production and ocular micromovements. Historically, ocular fluid mechanics studies can be traced back several centuries, with earlier descriptions of intraocular pressure and aqueous humour being credited to anatomists like Galen and Alhazen "the father of modern optics". Due to technological limitations of their time, their advancements were mainly observational. Quantitative studies of the eye structure and intraocular pressure started in the early 19th century, with Donders' research in 1862 establishing the first physiological relationships between ocular fluid pressure and quality of vision, as reviewed by Chaudhari *et al.* [7]. By the 20th century, the development and use of the Goldmann applanation tonometer added quantification of intraocular pressure to clinical practice, resulting in a broader understanding of ocular fluid dynamics. Mathematical modelling of eye physiology started to develop in the late 20th century, and with the advent of digital computing tools in the 1970s and 80s, the principles of fluid dynamics were applied to ocular structures. Ethier et al.'s [5]

overview is one of the most cited modern studies, covering the role of biomechanics in glaucoma pathophysiology and emphasizing the importance of modelling the resistance of outflow. In more recent years, CFD has enhanced the realism of simulations of AH circulation, as described by Fitt and Gonzalez [3], Villamarin et al. [6] etc. Murgoitio-Esandi et al. [1] used a coupled Darcy-Stokes model for the simulation of aqueous humour flow in glaucoma due to angle closure. The nonlinear rise in intra ocular pressure (IOP) when angle of outflow is obstructed above 180˚, highlighted the role of trabecular meshwork resistance. An advection-diffusion framework was also used to model solute transport, and their findings guide my use of pressure boundary conditions and the representation of porous media representation. These works are reflective of a shift from experimental assumptions to geometry-specific modelling. Today, the use of CFD is not only academic but also for the design of intraocular drug delivery systems, glaucoma implants and for predicting the outcomes of surgical procedures. Research in ocular fluids continues to progress into more detailed anatomical models, real-time simulations and multi-physics coupling.

AH circulation is usually in a vortex-like path, particularly in the anterior chamber where the corneal and iris geometries determine the direction of flow [6]. These patterns are sensitive to the geometry of the anterior chamber and that the location of inlets and state of outflow channels are also important. Under healthy conditions, flow of AH is symmetric and laminar. Whereas, in glaucomatous conditions, the narrowed drainage angles cause asymmetric velocity profiles and stagnation zones. The introduction of temperature or solute gradients introduces more complexity and as discussed in [1] thermally induced buoyancy can lead to secondary circulations. In addition, drug transport is mainly governed by the Péclet number and resulting concentration gradients. Fluid structure interaction (FSI) may also be critical in improved accuracy since elevated pressure may cause compliant boundaries such as the iris to deform [4] and the use of an Arbitrary Lagrangian-Eulerian (ALE) method highlighted the importance of coupling in the accuracy of the prediction of tissue response to fluid load.

Motivated by further exploring diseased eye fluid flows, this article focuses on simulating the flow of the aqueous humour in both healthy and glaucomatous eyes using ANSYS FLUENT CFD finite volume method software [8], considering a simplified 2D geometry of the eye anterior chamber. Using this method, the study seeks to provide comprehensive visualization of velocity patterns, distribution of pressure and wall shear stresses to support clinical and industrial innovations. The posterior chamber and vitreous humour are excluded, while the flow is assumed to be laminar, incompressible and Newtonian. Pulsating influences like blinking and fluctuations due to increased heart beating are also not considered. Although thermal gradients can be present in the eye, (such as corneal cooling), but due to computational power limitations, this study assumes isothermal conditions. Although we consider only 2-D simulations, a solid platform is stablished for future extensions to 3-D flows.

2. Modelling and Flow Physics

The human eye is a small, multi-chambered, intricately designed organ used for sustained optical function and internal homeostasis. It comprises the anterior and posterior chambers and the vitreous body. The anterior chamber which is the object of focus for this study, is bounded by the cornea in front and the iris and lens behind. It is filled with aqueous humour – the clear watery fluid responsible for the regulation of intraocular pressure and metabolic balance. The anterior segment contains the aqueous pathway and drainage structures. The cornea, iris and lens combined, are the defining structures of the anterior chamber geometry, while the ciliary body and processes are located behind the iris, where AH is produced (Fig. 1). The iridocorneal angle contains the trabecular meshwork and Schlemm's canal, making up the conventional route of drainage. An auxiliary outflow channel is provided by the uveoscleral pathway, which runs through the ciliary muscle and sclera.

Aqueous humour is released by the ciliary epithelium through its active transport mechanisms and ultrafiltration. In cyclic movements, it enters through the posterior chamber, flows through the pupil to the anterior chamber and exits through two main pathways.

- Conventional pathway: Through the trabecular meshwork, Schlemm's canal, collector channels and episcleral veins.
- Uveoscleral pathway: Through the ciliary muscle into the suprachoroidal space.

AH is used to maintain intraocular pressure, provide nutrients to the avascular lens and cornea, and remove metabolic waste from the anterior chamber. Normal IOP ranges from 10 to 21 mmHg and disturbances in outflow, mainly the TM, cause elevations in IOP, possibly leading to glaucomatous optic neuropathy. In open angle glaucoma (OAP), TM resistance increases slowly, while in angle-closure glaucoma (ACG), the peripheral iris obstructs the angle of drainage totally, leading to sudden pressure elevation [1].

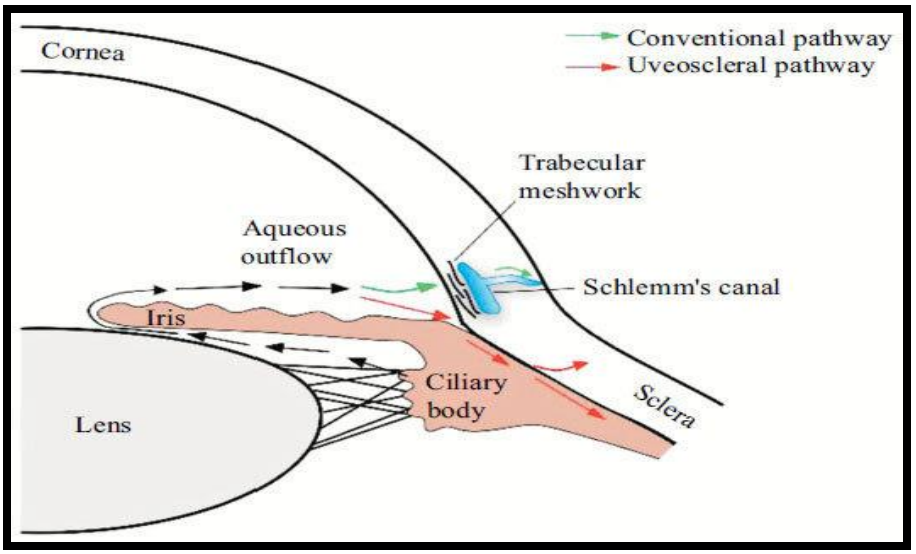

Figure 1:Outflow Pathway for AH

In the anterior chamber, the depth, angle width and iris-to-lens configuration varies in humans and with increasing age, flow behaviour is affected. Shallower chambers and narrower angles are high risk factors of angle closure problems. Issarti *et al.* [4] have stressed the importance of anatomical detail in designs, proving that alterations in pressure profiles were prevalent in finite element models where the modification of iris and lens geometries were carried out. AH is modelled in this study as a Newtonian, incompressible fluid under physiological conditions. It is assumed to share thermophysical properties with water, including a density of ~1000 kg/m3 and dynamic viscosity of ~0.001 Pa-s [3]. Flow of AH occurs in the low Reynolds number region of Re < 1, indicative of laminar, highly viscous flow regime. We adopt the approach of Murgoitio-Esandi *et al.* [1] who modelled aqueous humour fluid dynamics using a merged version of the Darcy-Stokes equations, accurately reflecting the porous nature of the trabecular meshwork. Through this formulation, the anterior chamber was modelled as a fluid region governed by the steady state version of Navier-Stokes equations, while the trabecular meshwork was considered as a porous domain governed by Darcy's Law. The flow of AH is mainly driven by the pressure gradient between the ciliary body and trabecular meshwork or uveoscleral pathway. In normal eyes, the intraocular pressure is within the range previously mentioned, but when considering glaucomatous eyes, the increased resistance leads to IOP elevation and optic nerve damage. 2-dimensional laminar AH fluid dynamics is governed by the 2-D Navier-Stokes equations i.e. mass conservation and momentum equations, in the absence of body forces [9-11]:

Continuity Equation:

$$\frac{\partial u}{\partial x}+\frac{\partial v}{\partial y}=0 \tag{1}$$

Momentum Equations (steady state version):

x-momentum

$$\rho\left[u\frac{\partial u}{\partial x}+v\frac{\partial u}{\partial y}\right]=-\frac{\partial p}{\partial x}+\mu\left[\frac{\partial^2 u}{\partial x^2}+\frac{\partial^2 u}{\partial y^2}\right] \tag{2}$$

y-momentum

$$\rho\left[u\frac{\partial v}{\partial x}+v\frac{\partial v}{\partial y}\right]=-\frac{\partial p}{\partial y}+\mu\left[\frac{\partial^2 v}{\partial x^2}+\frac{\partial^2 v}{\partial y^2}\right] \tag{3}$$

Here ρ is the fluid density (kg/m^3), μ is the dynamic viscosity (kgm/s), u and v are x and y-direction velocity components (m/s), p represents the pressure (Pa), F is a body force. The trabecular meshwork contains porous zones, which are governed by Darcy's law:

$$v = -\left(\frac{K}{\mu}\right)\nabla p \tag{4}$$

Here K (m^2) is the permeability of the trabecular meshwork. To accurately represent the eye in a CFD simulation, an anatomically and physiologically precise geometry must be used. As the anterior chamber is the primary circulation area of AH, the geometry used in this study was recreated in 2D from a full 3D model given in [1]. This decision also preserves computational efficiency and biomechanical accuracy. In the model developed in this work, we include a simplified representation of the ciliary region, trabecular meshwork and aqueous inflow region. Only a quarter section of the anterior chamber has been designed in this study. Following the work of [1] and Villamarin *et al.* [6], the anatomical model of the eye was cut along the vertical plane to reduce it to a symmetrical 2D profile. Structures such as the vitreous body, retina and optic nerves were removed as their effects are negligible. Relevant structures such as the site of AH production, the ciliary body; the anterior chamber bounded by the posterior part of the cornea; Schlemm's canal and trabecular meshwork, modelled as porous zones; and the pupil interface used as the main path of flow continuity, were retained. In an effort to reduce the complexity of meshing and unwanted extreme curvature resolution, the cornea was idealised as a circular arc as discussed by Ethier et al. [5], while the iris-lens junction was simplified into an angular interface. The geometry was created in ANSYS DesignModeler, as shown in Fig. 2. Following [1], [4] and [6], we deploy the following assumptions:

- The anterior geometry of the eye is symmetrical – this is justified by the sagittal mirror symmetry of the eye when observed in a cross-section view.
- The walls of the eye are rigid (FSI exclusion) – there is no deformation of the cornea or iris.
- The inflow is considered as directly from the ciliary body to the anterior chamber – posterior flow neglected.
- Porous outlet – the Schlemm's canal is represented as a porous region governed by the Darcy-formulated resistance.
- Steady state, laminar flow regime – this is based on the Reynolds numbers less than 1 reported across all AH referenced simulations.
- Only open-angle glaucoma is being considered – the flow velocity of aqueous humour is constant in open-angle glaucoma, and the severity of the condition is observed through the porous resistance of the trabecular meshwork, causing increased intraocular pressure in the chamber.

The use of these assumptions improves solver stability, while maintaining the flow characteristics observed in empirical studies [3, 5].

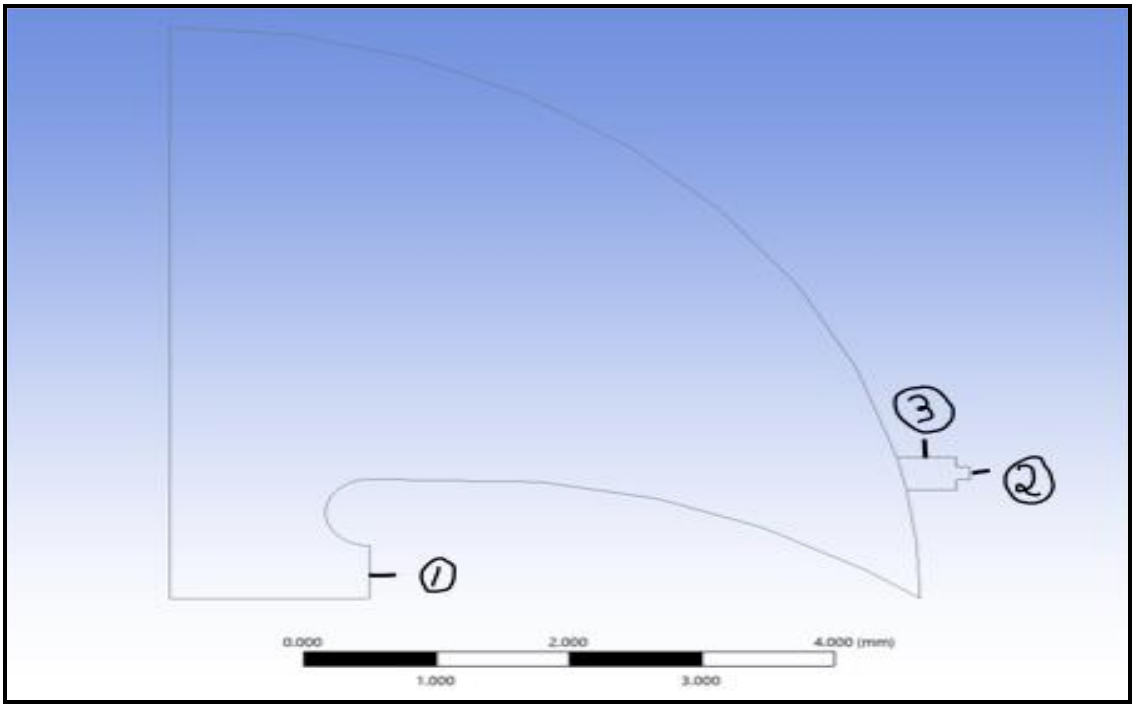

Figure 2. Simplified model for the anterior chamber. (1) Aqueous humour inlet region (2) Outflow boundary of aqueous humour (3) Trabecular meshwork - porous region.

2.1 Boundary Conditions

The use of boundary conditions in CFD improve solver stability and the realism of the simulated study. Here, the anterior chamber was treated as a pressure-driven cavity where AH enters from the ciliary body and exits through the trabecular meshwork, according to Darcy's law.

2.1.1 Ciliary Zone - Inlet

A velocity inlet was used based on a calculated velocity of 6.9e-5 m/s using the formula below.

$$V = \frac{Q}{A}, A = h \times 1\ (unit\ depth) = 0.6 \times 10^{-3} m^2, V = \frac{4.17 \times 10^{-11}}{0.6 \times 10^{-3}} = 6.94 \times 10^{-5} m/s \quad (5)$$

Inlet flow rate was assumed to be 2.5μL/min = 4.17e-11 m^3/s [1, 5] while temperature was neglected as thermal effects were not considered. A uniform velocity profile at the inlet was also assumed.

2.1.2 Trabecular Meshwork - Outlet

A pressure outlet boundary type was chosen for this section, with an expected pressure drop of 5-7mmHg in healthy eyes and about 20mmHg in glaucomatous eyes, as observed in [1]. Resistance values were calibrated from Ethier *et al.* [5].

2.1.3 Wall conditions

A no-slip wall condition was used, with no thermal conditions considered.

3. Ansys Simple Numerical Solution and Material Data

Considering the laminar characteristics and low velocity of AH, turbulent models are not required. The laminar solver is used. The most common pressure-velocity algorithm is the SIMPLE (Semi-Implicit Pressure-Linked Equation) algorithm. A brief breakdown of the SIMPLE algorithm is given below. The SIMPLE algorithm works by assuming an initial pressure field, proceeding to solve the momentum equations using the pressure assumed and deriving a correction equation from the continuity equation. The pressure and velocity fields are updated and solved iteratively until convergence is achieved. The flowchart in **Fig. 3** below provides insight to the SIMPLE algorithm [8].

This method is known for its stability and widely acceptable quality of results. It is a popular approach in CFD studies in biofluid dynamics and handles incompressible flows very accurately.

3.1 Tabulated Fluid Properties and Parameters for Simulation

Tables 1 and 2 below document the key differences between the flow parameters, for the two cases of healthy physiological and glaucomatous eyes and are utilized for simulation settings in ANSYS Fluent.

Table 1: Simulation Parameters for the Healthy Eye

Parameters	Value	Unit	Source
Density	1000	Kg/m^3	Villamarin *et al.* [6]
Dynamic Viscosity	0.001	Pa.s	Villamarin *et al.* [6]
Inlet Flow Rate	2.5	μL/min	Murgoitio-Esandi *et al.* [1]
IOP	15	mmHg	Ethier *et al.* [5]

Table 2: Simulation Parameters for Glaucomatous Eye

Parameters	Value	Unit	Source
Density	1000	Kg/m^3	Same as healthy eye
Dynamic Viscosity	0.001	Pa.s	Same as healthy eye
Inlet Flow Rate	2.5	μL/min	Murgoitio-Esandi *et al.* [1]
IOP	25-30	mmHg	Murgoitio-Esandi *et al.* [1]

4. Ansys Fluent CFD Methodology

4.1 Geometric Considerations

The anterior chamber geometry for this study was inspired by the quarter circular model used by Murguitio Esandi *et al.* [1]. An absence of literature surrounding ocular research contributed to the decision of drafting a simpler geometry. Here, the eye model was simplified to a 2D quarter circle, closely resembling the general shape of the human eye. Although this model is greatly simplified, it gives the opportunity for a focus on the physiological properties of aqueous humour, while creating a baseline to produce more detailed geometries for further simulations. Dautriche *et al.* [12] successfully implemented and analysed ocular fluid transport using a simplified model of the eye, and other similar studies have shown the usefulness of model reduction in complex design cases. Computational modelling of aqueous humour dynamics requires careful geometric considerations, enabling the preservation of physiological integrity of intraocular flow. The reduced approach taken in the geometry formation is backed by the research practices observed in CFD studies such as Basson *et al.* [13] and Johnson *et al.* [14], where

symmetry conditions were assumed in anatomical axes to allow for computational efficiency without reduction in accuracy. The geometry constructed comprised of key anatomical areas for the simulation of aqueous humour flow, i.e., the ciliary body inflow region, central anterior chamber and trabecular meshwork serving as the conventional outflow pathway. Regions included in the geometry were included based on their impact on AH pressure-velocity field and the resistance mechanisms governing intraocular pressure. Table 3 summarizes the components of the model geometry.

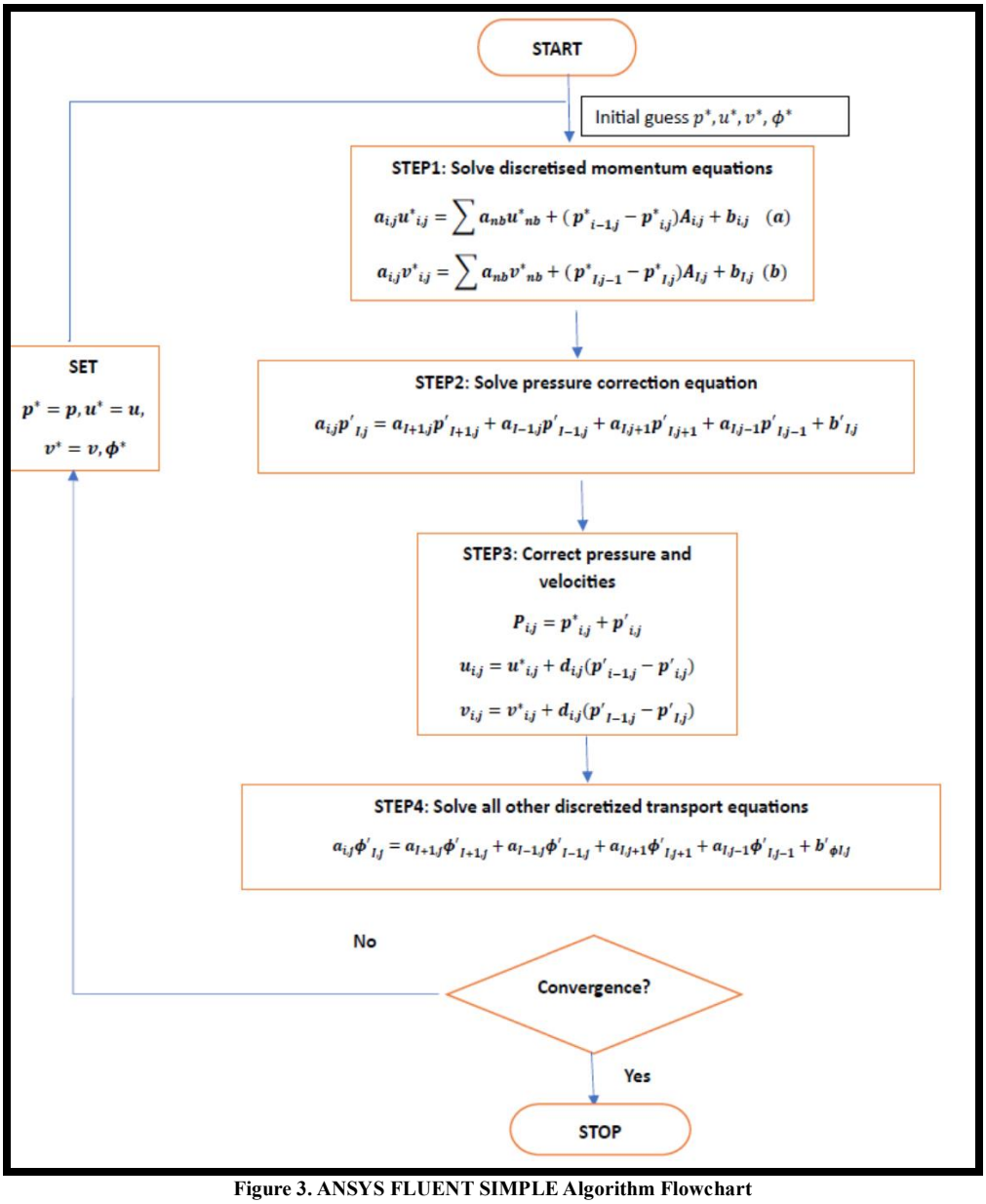

Figure 3. ANSYS FLUENT SIMPLE Algorithm Flowchart

The ciliary region is the primary inflow area for aqueous humour, modelled with a defined velocity inlet derived from the clinical production rates discussed in previous publications, which range from 2.4-3 μL/min in healthy eyes. The value was then adjusted using the cross-sectional area approximations [6]. A key regulator of IOP, the trabecular meshwork, was modelled as a porous zone using the values of permeability reported in literature cited in previous chapters, as ranging from 2e-15 to e-15 m^2 in healthy eyes, and 2.9e-16 m^2 for glaucomatous eyes [13]. The geometric discretisation used in this study allows the flow convergence around the trabecular meshwork to reflect an accurate pressure build-up needed to validate the results against previous bodies of work in healthy and pathological eyes. The model of the anterior chamber was constructed in ANSYS DesignModeler 2024 R2. Geometry creation, edge splitting, zone isolation and face assignments for porous media was carried out in the modeller environment to

avoid compatibility issues with meshing and fluent solver settings. A closed loop sketch was required to enable a surface generation command to be executed from the profile curve, ensuring that the downstream meshing operations could successfully generate the surface and volume elements required. The geometry consists of a concave anterior curvature representing the corneal dome and a narrowed outflow slit representing the trabecular meshwork. Edge splitting was used to assign a porous boundary, to allow the simulation of outflow resistance in setup stages. Although some difficulty was encountered in the selection of faces for "named selections", these were resolved by projecting lines and splitting faces, resulting in the isolation of the TM interface without mesh distortion. Figure 4 shows the geometry highlighting the inlet, interior fluid zone and trabecular meshwork as porous face.

Table 3: Core Regions of the Geometry and Relevance in Simulation

Geometric Feature	Present in Model	Functionality in Simulation
Ciliary Body	Yes	AH inlet region (modelled through inlet boundary conditions).
Central Anterior Chamber	Yes	Primary flow domain.
Trabecular Meshwork	Yes	Modelled as a porous zone to simulate outflow resistance.
Schlemm's Canal	No	Negligible in the context of the simulation. Its function was captured through the TM's porous outlet setting.
Corneal Surface	Yes	Useful for wall shear stress analysis and contour mapping.
Lens and Iris	No (simplified)	Implicitly represented by curvature and boundary walls.

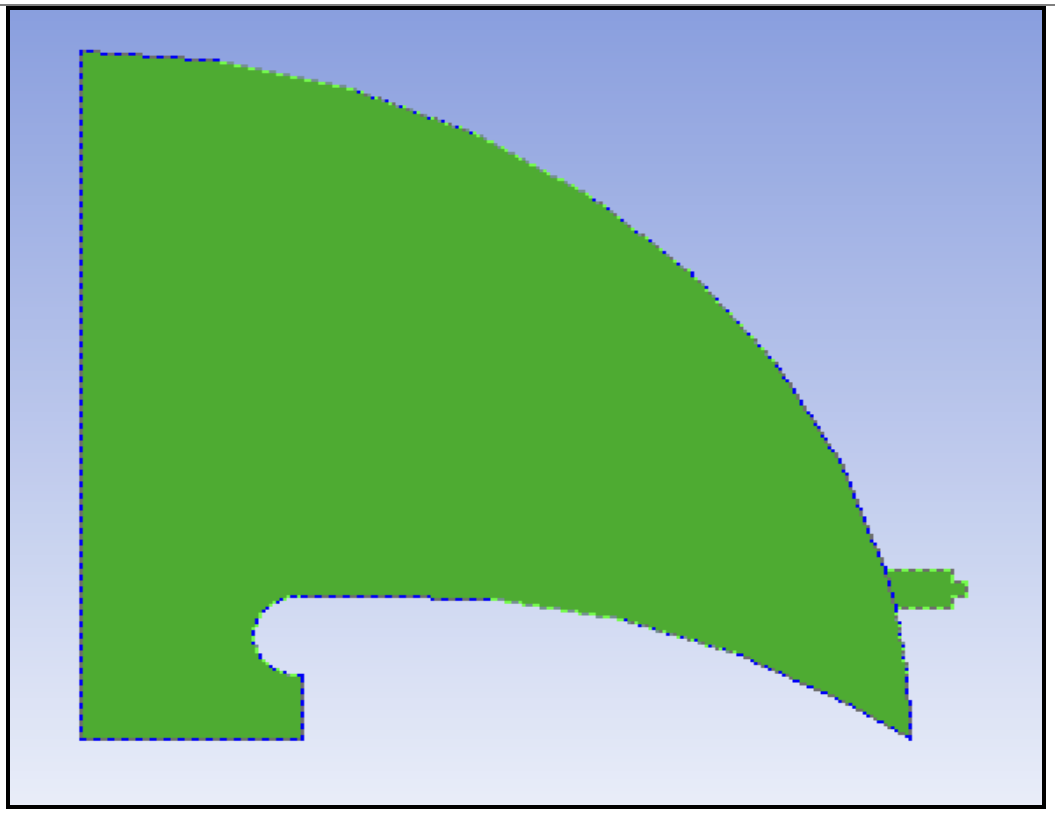

Figure 4: ANSYS FLUENT closed sketch with surface representing anterior chamber.

Although a full 3D model of the anterior chamber would have provided more physiological complexity, previous literature indicates that the quarter symmetry method sufficiently captures the required pressure gradients and streamline behaviour within the boundaries of the study. This simplified method also contributes to the speed of convergence and solver stability. The importance of Schlemm's canal and connector channels cannot be overstated, however, in this study, they were not modelled explicitly and instead were substituted with the use of a porous zone, consistent with previous studies [13].

4.2 Meshing

Mesh generation and accuracy is an essential part of every CFD simulation, allowing the capture of physiologically meaningful flow behaviour in the anterior chamber. Given the fine flow gradients in the trabecular mesh (TM) area and inlet region, mesh settings must be adequate to resolve these areas without excessive skewness. To achieve this, a structured mesh strategy was adopted using a combination of system-assigned and user-defined refinement controls. The base mesh resolution was set using ANSYS' predefined "fine" sizing, while edge sizing was applied to the outlet and inlet zones where mesh concentrations in regions where high velocity gradients are expected, is to be prioritised. We opted for the following: Number of elements: 3350, Number of nodes: 3351 and Skewness: <0.25. Fig. 5 shows the finalized surface body mesh.

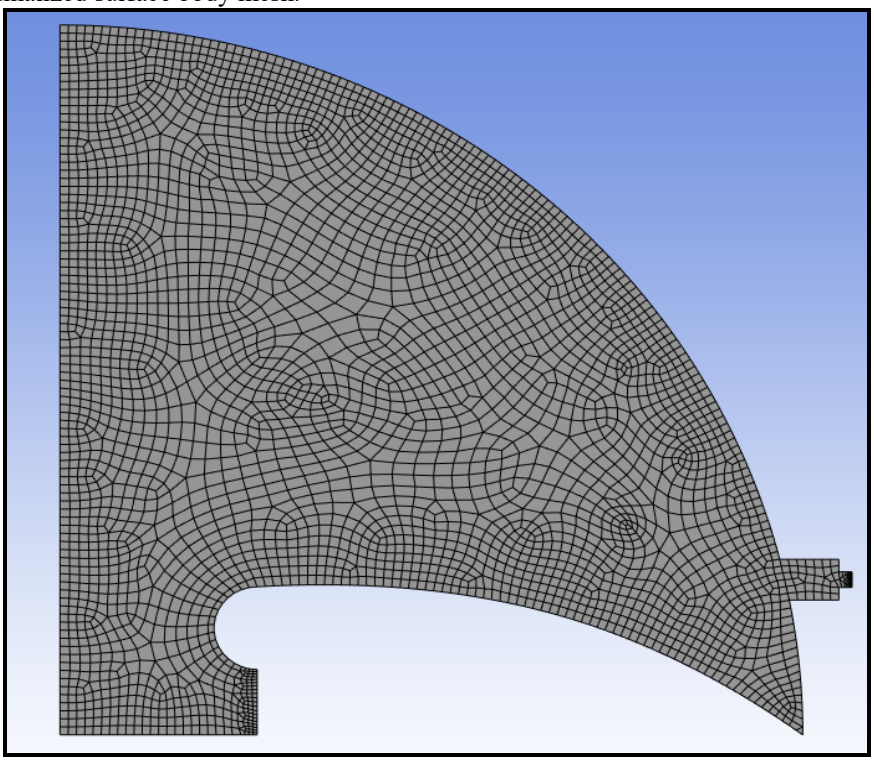

Figure 5. Meshed view of surface body.

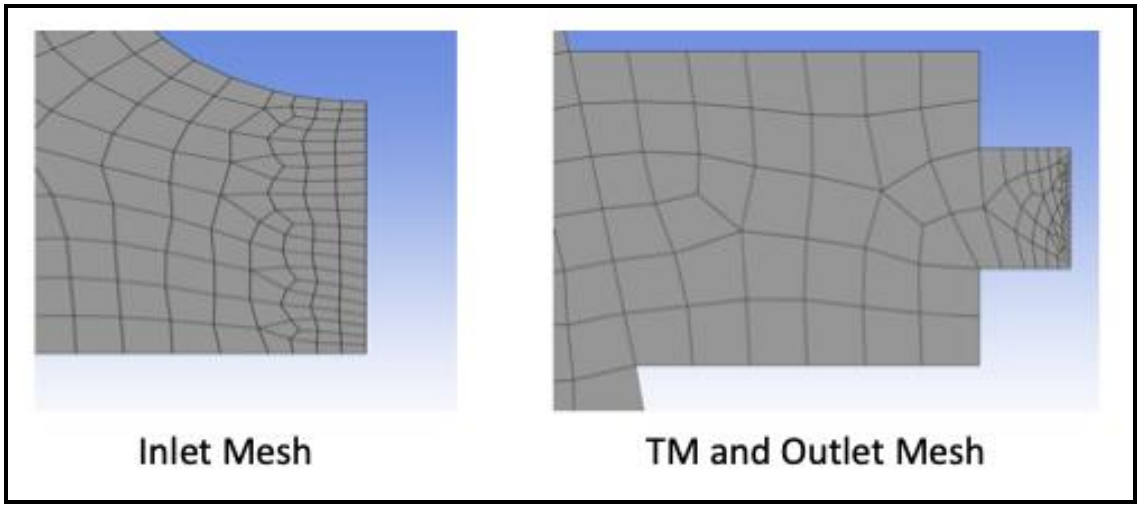

Figure 6. Inlet and Outlet mesh views.

The named selections were verified to have transferred correctly. Due to grid quality considerations, the mesh was evaluated for skewness, orthogonal quality and aspect ratio. Using ANSYS recommendations, skewness was minimised to < 0.25, orthogonal quality > 0.85 and aspect ratio < 5.

4.3 Solver Setup and Simulation Settings

The solver setup is used to define the numerical implementation process for the equations governing the motion of fluids within the anterior chamber. This includes the material properties, boundary conditions, flow physics (laminar), porous media characteristics and solution methods. Double precision was enabled to improve the numerical accuracy of Navier-Stokes equations solving. Parallel processing allows computation speed boosts through the distribution of the computational workload across multiple processors. Due to the computational power of the computer in use during the simulation, 15 parallel processors were selected, to ensure fast mesh convergence and minimal grid distortion. The 2-D steady, viscous, laminar pressure-based flow solver is used. The pressure-based solver is best for incompressible, laminar flows hence the selection choice. Time setting was set to steady, as no transient effects were considered for this study. The choice of a viscous laminar model is validated by literature [1-6], as aqueous humour flow is known to be laminar within the Reynold's number range of < 1. Energy equations were turned off, as thermal effects are not considered in this study. The conditions of flow are assumed to be isothermal under normal physiological settings.

4.4 Material Creation

AH is defined as a new material in the fluid library with density (1000 kg/m^3) and dynamic viscosity (0.001 Pa.s).

4.5 Cell Zone Conditions

The trabecular meshwork was modelled as a porous region to accurately depict its function as a drainage route for aqueous humour leaving the anterior chamber. This setting can be enabled through the steps below. In the "cell zone conditions" we specify porous zone with Viscous resistance (2.43 x 10^{13} m^{-2}) and Inertial resistance (0). While simulating glaucomatous conditions, the viscous resistance was increased to 6.5 x 10^{13} m^{-2} and inertial resistance maintained at 0, which is the applicable condition when form drag in low velocity flows is negligible. These resistance values were derived from the interpretation of permeability ranges reported in [5] and fine-tuned to be compatible with the selected simulation settings and expected pressure gradients in the anterior chamber for both healthy and glaucomatous cases. Further cases were simulated to verify the conformity of the two main cases to published literature.

4.6 Boundary Conditions

To set boundary conditions (inlet and outlet), we prescribe (Velocity inlet) > Magnitude (6.94 x 10^{-5} m/s) and Outlet > Type (Pressure outlet) > Gauge pressure (0 Pa). Wall motion is prescribed as (Stationary). Shear condition is set as (no-slip). The velocity magnitude at the inlet was computed from an inflow rate of 2.5uL/min and an inlet area based on the geometry height of 0.6mm. Guage pressure of 0 Pa supports the assumption of open drainage into a reservoir (episcleral veins) at atmospheric pressure, allowing ANSYS to automatically calculate the pressure in the chamber as the conditions change. Wall conditions were set to reflect the no-slip conditions of the corneal and scleral boundaries.

4.7 Solution Methods and Controls

We select from Solution methods, "SIMPLE" with "Spatial Discretization", "Gradient", "Least squares cell based", "Pressure", "Standard", "Momentum" and "Second order upwind". The SIMPLE scheme is very accurate for laminar viscous flow simulation. The least squares cell based gradient setting ensures accuracy in the calculation of spatial derivatives in calculations, while the second order upwind momentum setting is an accuracy-improving setting for reducing the numerical diffusion of the solution. Under Solution controls, we select Pressure (0.3), Momentum (0.7), Body forces (1). These settings ensure that the divergence and oscillations in the pressure field remain minimal, while balancing the convergence speed of the simulation with stability. They are widely recommended in ocular research literature and were kept constant, for all cases to ensure consistency in comparisons. 1000 iterations are prescribed. Simulations converged within 200 to 300 iterations with residuals monitored for continuity and velocity components, with convergence criteria set to all residuals < 10^{-5}. No timestep was introduced, as the study was considered steady state.

4.8 Mesh Independence Study

Due to the critical role of mesh quality on the results of CFD simulations, it is of utmost importance to conduct a mesh independence test to confirm the correctness of the underlying physiological considerations without compromising the results of a simulation due to size of mesh. To conduct this test, multiple simulations were carried out using different mesh settings (simulation number S/N) and compared to the maximum intraocular pressure in the healthy case scenario, which served as the baseline for further simulations.

As seen in Table 4 and Fig. 7, the margin of error between the pressures observed using the smallest and finest mesh resolutions is less than 5%, indicating that further changes to the mesh will yield negligible differences. A slight overprediction of pressure at lower mesh densities can be observed in the above trend, which is expected as it is an indication of lower resolution in critical areas such as the porous trabecular meshwork region. The baseline mesh yields a result very close to the range seen in previously cited research, and this mesh study validates the independence of the mesh settings used to carry out the simulations.

Table 4: Mesh Independence Test Values

S/N	No. of Elements	Max Pressure (KPa)	Max Pressure (mmHg)
1.	2804	2.06	15.53
2.	3123	2.05	15.33
3.	3350	2.01	15.08
4.	3598	2.00	15.00
5.	3924	1.98	14.91
6.	4199	1.99	14.93

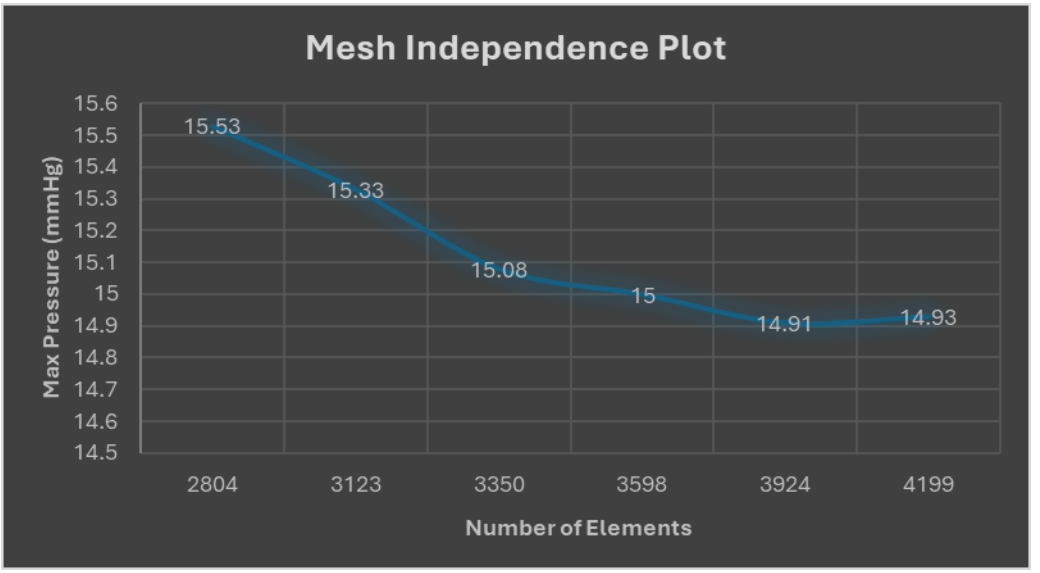

Figure 7. Mesh independence plot

5. Ansys Fluent CFD Simulation Results and Discussion

Based on Table 1, a range of simulations is conducted for different healthy and diseased cases for the anterior chamber of the eye. The results of each case have been examined in detail below, focusing on static pressure distributions (intraocular pressure), velocity fields, vorticity magnitudes and behaviour of residuals in convergence. First presented, is the *healthy eye case*, which was used as a baseline for the entire study, followed by the *glaucomatous case* and three further additional cases with parametric variations. The results are compared with previous numerical and experimental ocular research studies to validate model behaviour.

5.1 Healthy Eye Case

5.1.1 Distribution of Static Pressure

The healthy anterior chamber with trabecular meshwork viscous resistance of 2.43 x 10^{13} m^{-2} produced a maximum static pressure of approximately 15.08mmHg (2.01 KPa) at the inlet region, decreasing with smoothness towards the outlet as shown in Figure 8. The colour gradient is almost uniformly red, indicative of a slow pressure-drop across the chamber. The spatial distribution of pressure aligns with the laminar nature of aqueous humour flow, as anticipated for low Reynolds number regimes. This trend aligns with the research of Ethier *et al.* [5] who observed minimal pressure fluctuations in the anterior chamber under healthy conditions, and Johnson *et al.* [14] who confirmed that physiological IOP levels are maintained through balanced in and outflow dynamics. Compared to Murgoitio-Esandi *et al.* [1] whose simulation produced an average anterior chamber IOP of 15.7 mmHg under similar inlet and TM permeability settings, this represents a 3.59% difference, indicating perfect alignment.

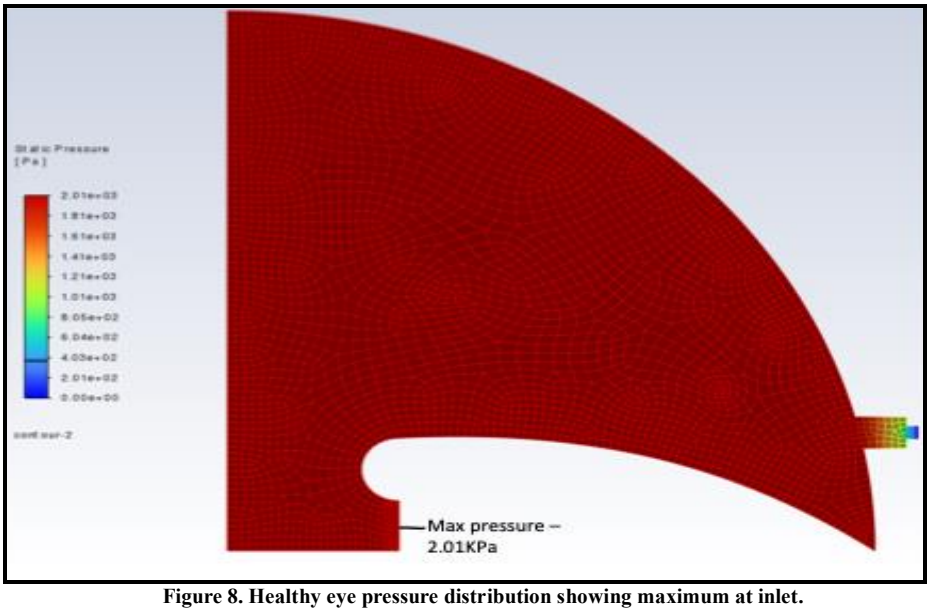

Figure 8. Healthy eye pressure distribution showing maximum at inlet.

5.1.2 Convergence Behaviour

The residual plots continuity, x-velocity and y-velocity shown in Figure 9 shows fast initial drops within the first 20 iterations, succeeded by a gradual decline to below 10^{-5} for velocity and continuity by the 130^{th} iteration. The convergence behaviour is smooth and does not show high oscillation, indicating good numerical stability. This behaviour is common for laminar flow under the SIMPLE scheme of pressure-velocity coupling, which ensures stable mass conservation.

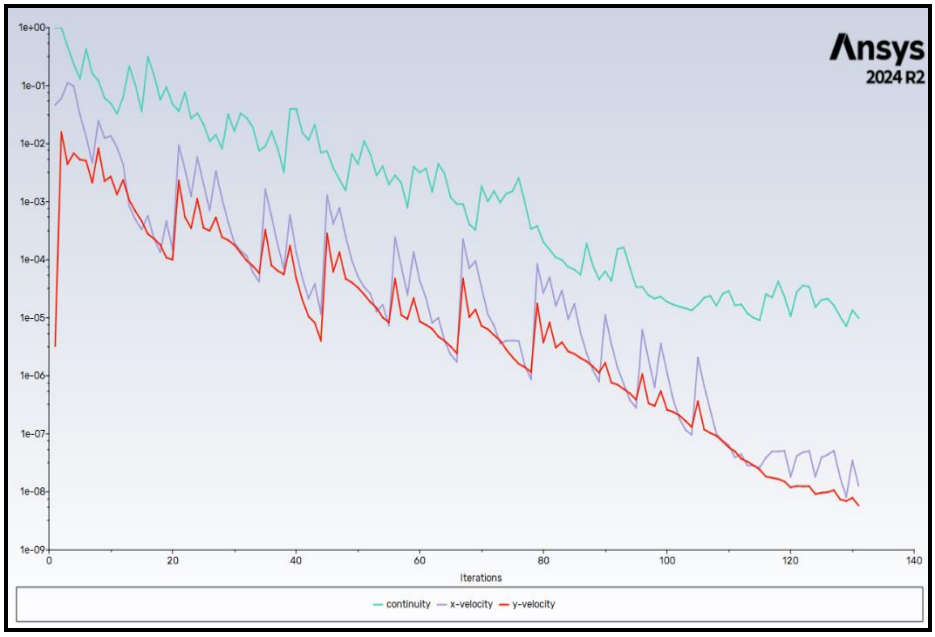

Figure 9. Convergence history healthy eye simulation showing steady decay of residuals.

5. 1.3 Velocity Field – Path lines

Velocity path lines shown in Figure 10 show a smooth arcuate trajectory from the ciliary body inlet towards the trabecular meshwork outlet, with slight curvature driven by the anatomical geometry. The maximum velocity magnitude observed was 2.89 x 10^{-4} m/s, at the outlet region where the increased pressure accelerates the fluid. The absence of significant recirculation agrees with the observations of Ooi and Ng [15], who deduced a predominantly unidirectional anterior chamber flow under steady-state conditions.

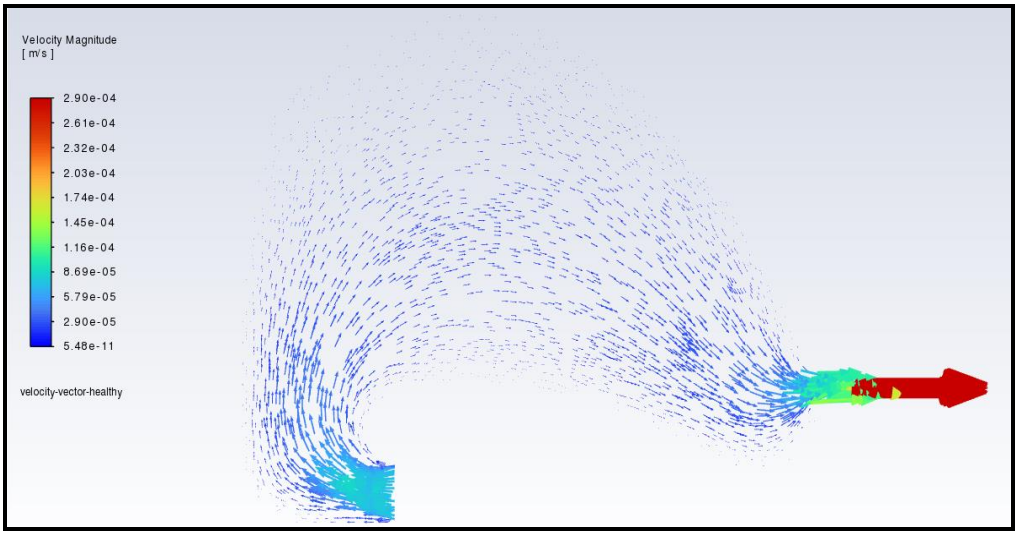

Figure 10: Velocity path lines in the healthy eye case showing smooth transition.

5.1.4 Velocity Field – Streamlines

Visualisation of streamlines (Fig. 11) confirms the laminarity of the flow, maintaining parallel spacing except near the outlet where acceleration caused an increase in line density. This indicates a low shear environment within the chamber, supporting minimal mechanical stress on intraocular tissues.

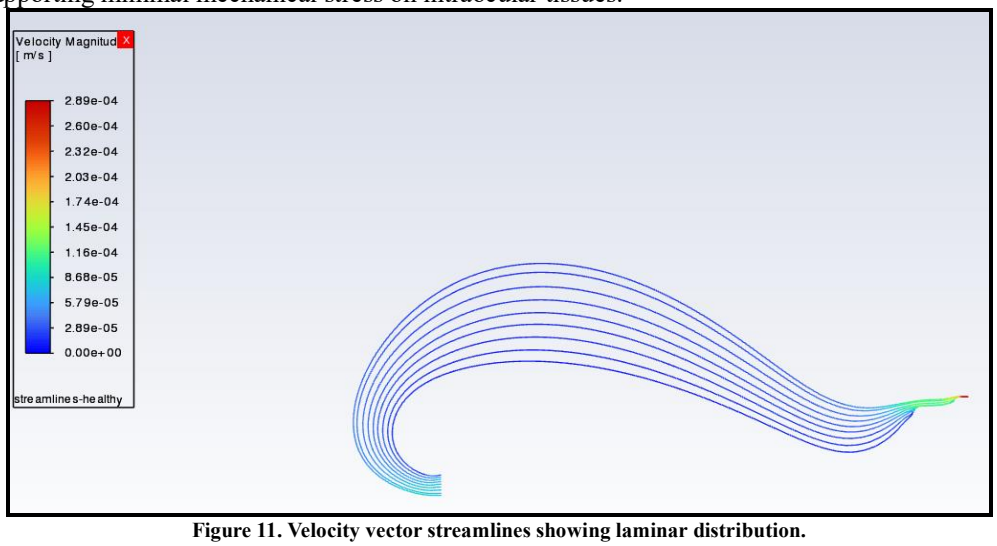

Figure 11. Velocity vector streamlines showing laminar distribution.

5.1.5 Vorticity Magnitude

The rotational activity shown in the vorticity plot (**Fig. 12**) is extremely low with a magnitude peaking at 3.31 x 10^{1} s^{-1} near the outlet. This is expected of low Reynolds flow which does not have anatomical obstructions. Low vorticity aligns with the research of Johnson *et al.* [14] who observed that significant vortex formation is usually associated with pathological resistance or pulsatile flow in the anterior chamber.

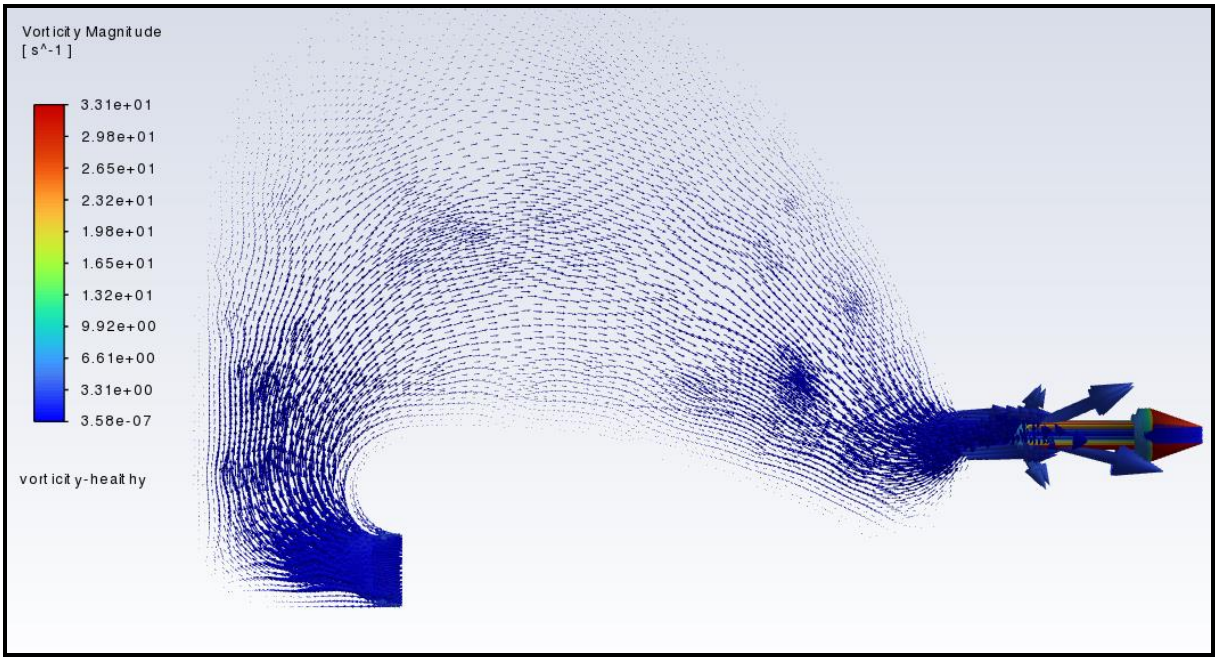

Figure 12. Vorticity for healthy eye highlighting minimal rotational flow.

5.2 Glaucomatous Eye Case

5.2.1 Distribution of Static Pressure

In the glaucomatous anterior chamber simulation with the trabecular meshwork resistance increased to 6.5 x 10^{13} m^{-2} resulted in a maximum static pressure (Fig. 13) of 40.42mmHg (5.39 KPa). This value is significantly higher than the physiological range for a healthy eye, which is 10-21mmHg, and falls exactly within the glaucomatous IOP range reported Ethier *et al.* [5] and represents a 2.82% difference compared to the 39.33 mmHg case reported by Heys and Barocas [16] for severely reduced outflow facility. This agreement in values reinforces the suitability of the porous media resistance value chosen for the glaucomatous case. The highest pressure is concentrated at the inlet-adjacent region and sustained across most of the anterior chamber, before dropping sharply at the TM outlet. This sustained IOP elevation is consistent with reduced aqueous humour drainage efficiency caused by the increased resistance of the porous TM.

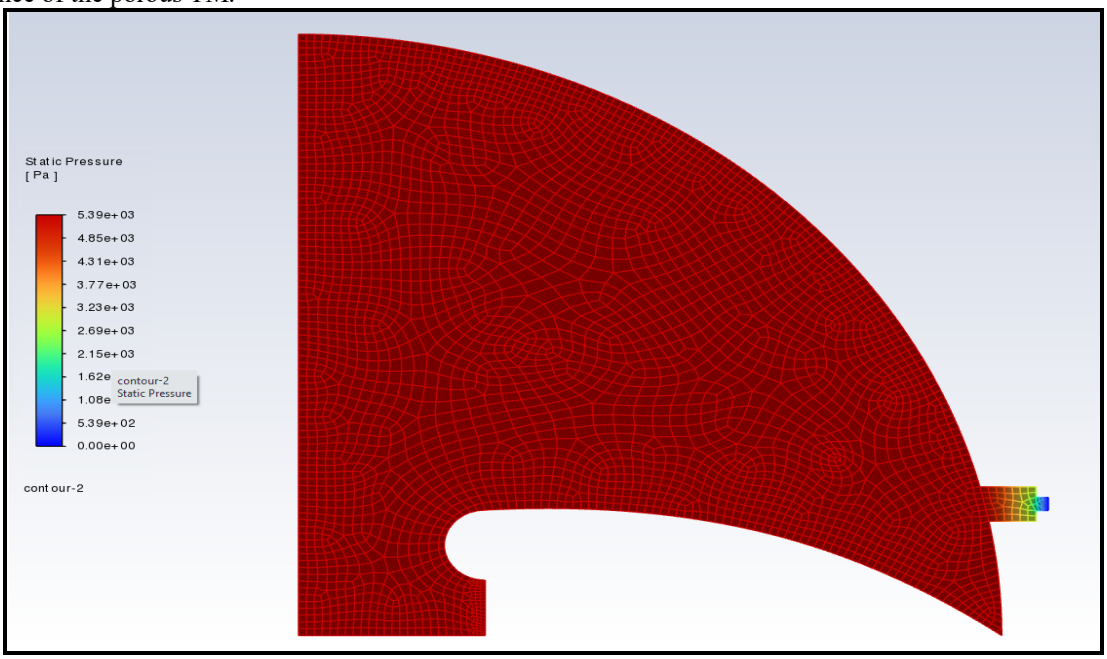

Figure 13. Static pressure contour for glaucomatous eye case, showing persistence of high pressure up to the TM outlet.

5.2.2 Convergence Analysis

The convergence trend of the glaucomatous eye simulation shows a similar decay pattern to the healthy case but shows a higher number of iterations to meet the set convergence criteria of 10^{-6} velocity residuals. The pronounced nature of its oscillations in the early phase is expected in high resistance porous media simulations where the solver requires adaptation to compute the steeper pressure gradients present in the chamber. This behaviour is consistent with the observation of Villamarin *et al.* [6] that higher outlet resistance in laminar incompressible flows leads to slower stabilisation of residuals. Figure 14 shows this behaviour.

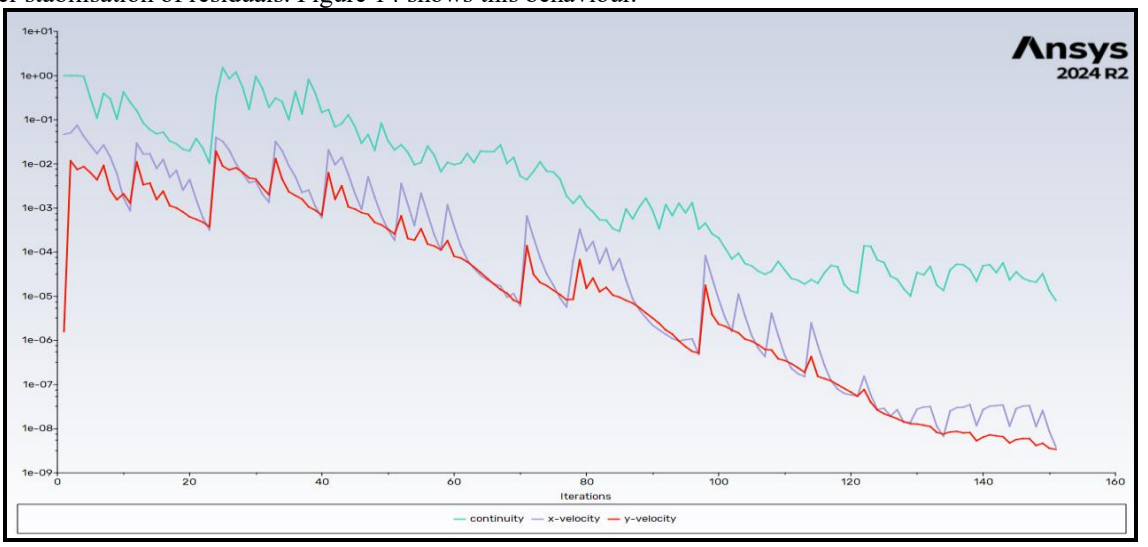

Figure 14. Convergence plot for glaucomatous case, showing more oscillatory decay.

5.2.3 Velocity Field – Pathlines

The path line visualisation in Figure 15 shows a similar trajectory to the healthy case but with denser velocity vectors concentrated near the outlet. The maximum velocity remains 2.89 x 10^{-4} m/s, unchanged from the healthy simulation due to the identical inlet conditions consistent with observed trends in open-angle glaucoma. However, the confinement of local acceleration spatially near the trabecular meshwork (TM) outlet is noticeable due to the constriction effect of the increased resistance in the TM area.

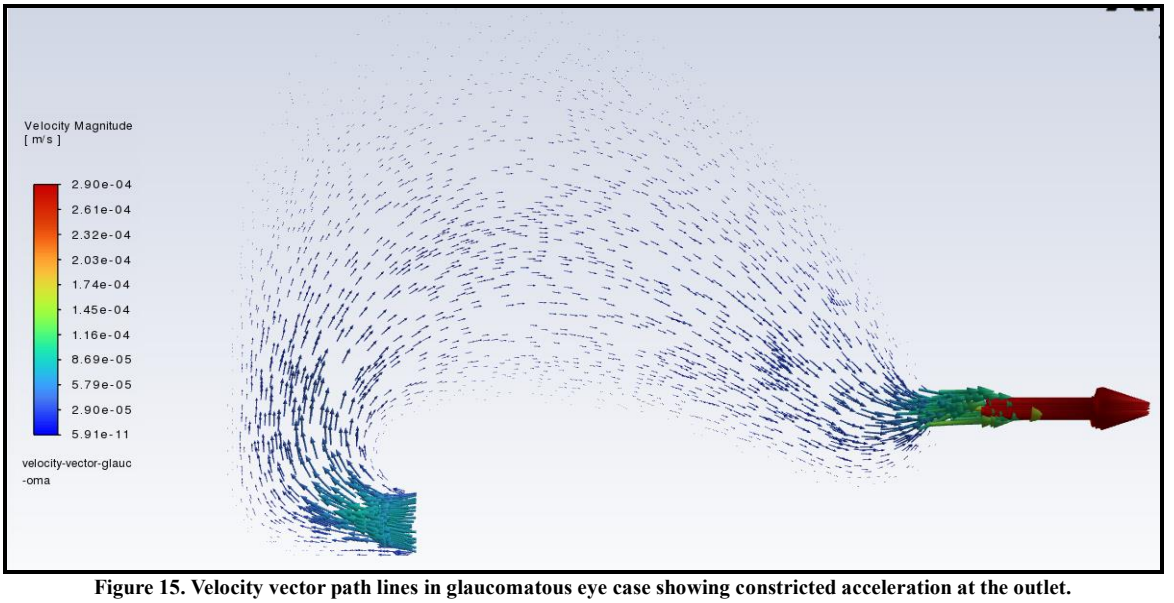

Figure 15. Velocity vector path lines in glaucomatous eye case showing constricted acceleration at the outlet.

5.2.4 Velocity Field – Streamlines

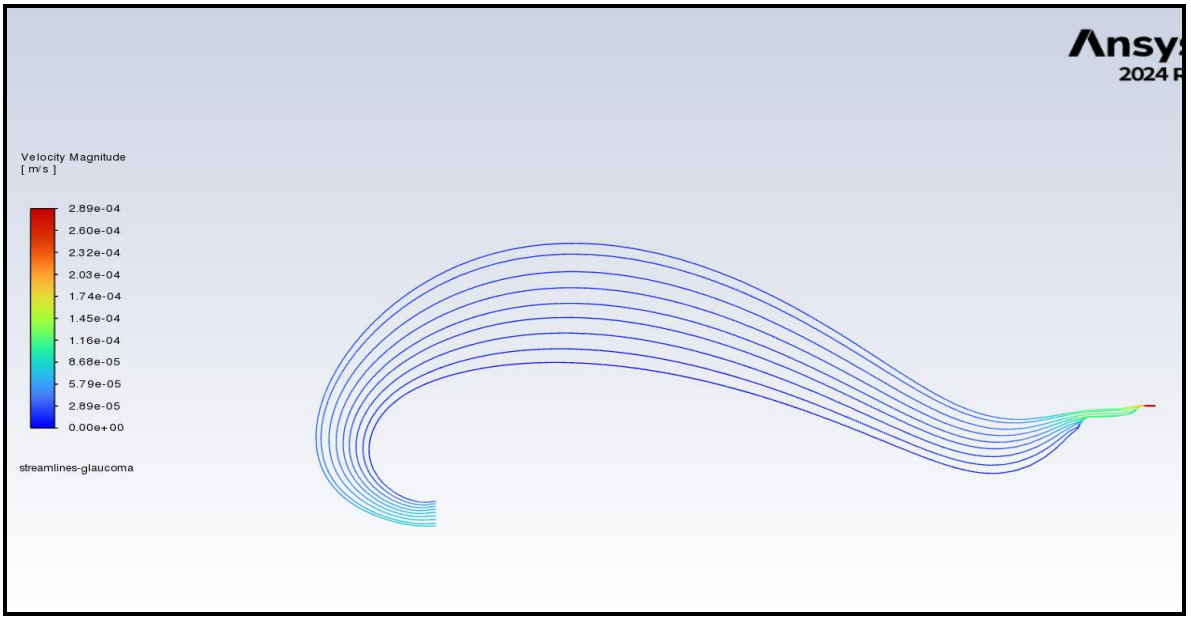

Figure 16. Flow streamlines for galucomatous case, with greater directional conversion at the outlet.

Streamlines shown in Figure 16 display the smooth laminar flow but with a noticeable convergence towards the outlet, as shown in the pathlines. This focused effect is due to the redistribution caused by elevated resistance and reduced drainage efficiency.

5.2.5 Magnitude of Vorticity

Fig. 17 below shows the vorticity field which maintains a maximum value of 3.31 x 10^{1} s^{-1}, but with high vorticity regions showing greater localisation around the TM outlet. This is an indicator of localised shear stresses devoid of large-scale recirculation. The research of Abu-Hassan *et al.* [17] showed a link between glaucomatous outflow restriction and micro-scale shear concentrations which is consistent with the localised shear observed in the vorticity vector plots and known to contribute to TM tissue damage.

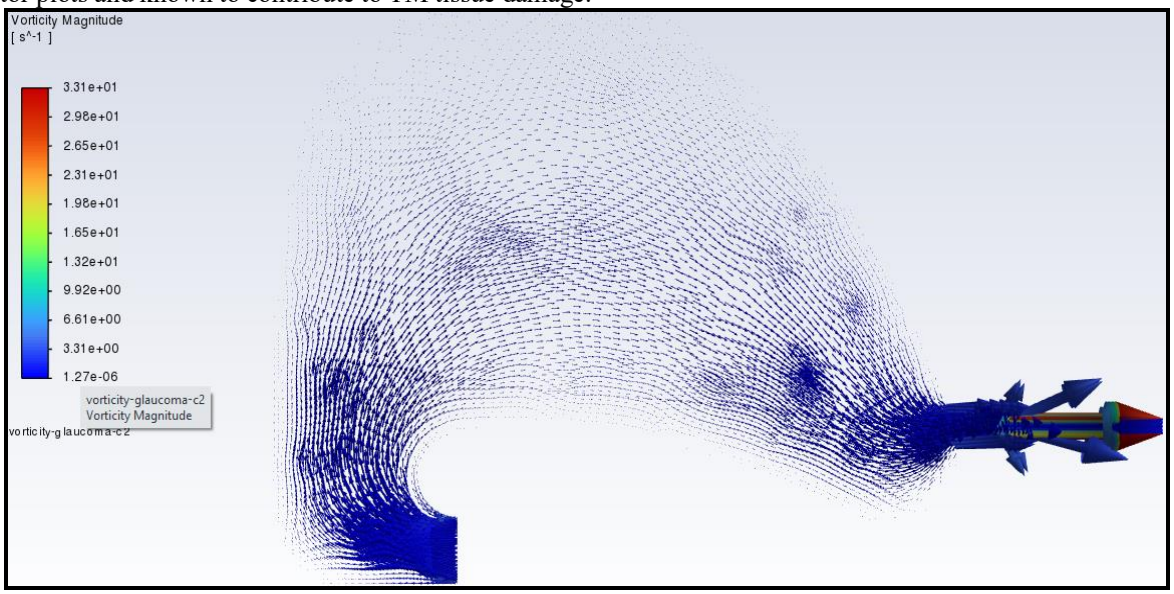

Figure 17. Vorticity magnitude showing slightly concentrated shear regions at the outlet.

5.3 Additional Cases (with porous outlet resistance variation)

5.3.1 Static Pressure Distribution

Three additional simulations have been conducted to provide additional cases for trend observation. In these cases, the resistance conditions of the porous outlet were altered to vary between intermediate and extreme glaucomatous conditions. The resulting maximum pressures spanned from 4.14 KPa to 7.46 KPa (i.e., 31 to 55.95 mmHg), corresponding *Cases 3, 4 and 5*, in Fig. 18, showing a clear relationship between trabecular meshwork resistance and sustained intraocular pressure. In all cases, the *high-pressure zone* originates from the ciliary inlet and translates throughout the chamber, dropping sharply at the trabecular meshwork and through the outlet. The magnitude and spatial persistence of the high-pressure region also increase with outlet resistance. This fluid behaviour is consistent with the observation of Heys and Barocas [16] who showed that doubling the resistance of the trabecular meshwork can cause an almost proportional elevation in steady-state IOP.

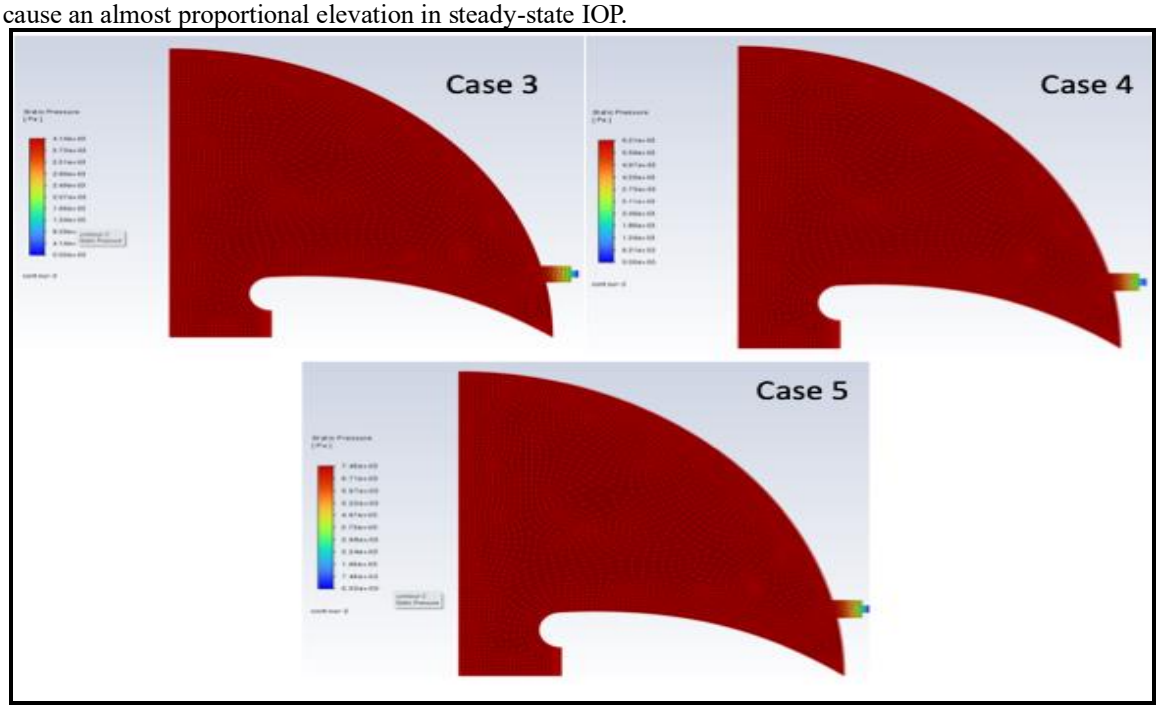

Figure 18: Comparative view of pressure contours for additional cases.

All cases converged to the residual velocity threshold of 10^{-5} but with differing iteration counts and varying oscillatory behaviour (Fig. 19). The lowest resistance case converged in about 140 iterations while the highest case required a little over 160 iterations to converge, mirroring the glaucomatous trend of prolonged solver stabilisation under steeper pressure gradients. Residual oscillations were more pronounced in the higher resistance cases, reflecting the sensitivity of the pressure-velocity coupling using SIMPLE algorithm, to the stronger outlet restrictions. This behaviour is confirmed by previously cited research and considered appropriate for this study.

5.3.3 Velocity Field – Pathlines

Despite variations in TM resistance, the maximum velocity stayed constant at 2.89×10^{-4} m/s due to identical inlet boundary conditions. Inlet velocity was maintained for all cases, as is known to be practical in open angle glaucoma, where the secretion rate of aqueous humour is unchanged. There is a very slightly noticeable change in the distribution of high velocity regions in the three cases (Fig. 20), with higher resistance cases showing concentration into a narrow jet immediately upstream of the TM region. This behaviour is confirmed by Tamm *et al.* [18] who reported jetting in trabecular meshwork models with high resistance.

5.3.2 Convergence Trends

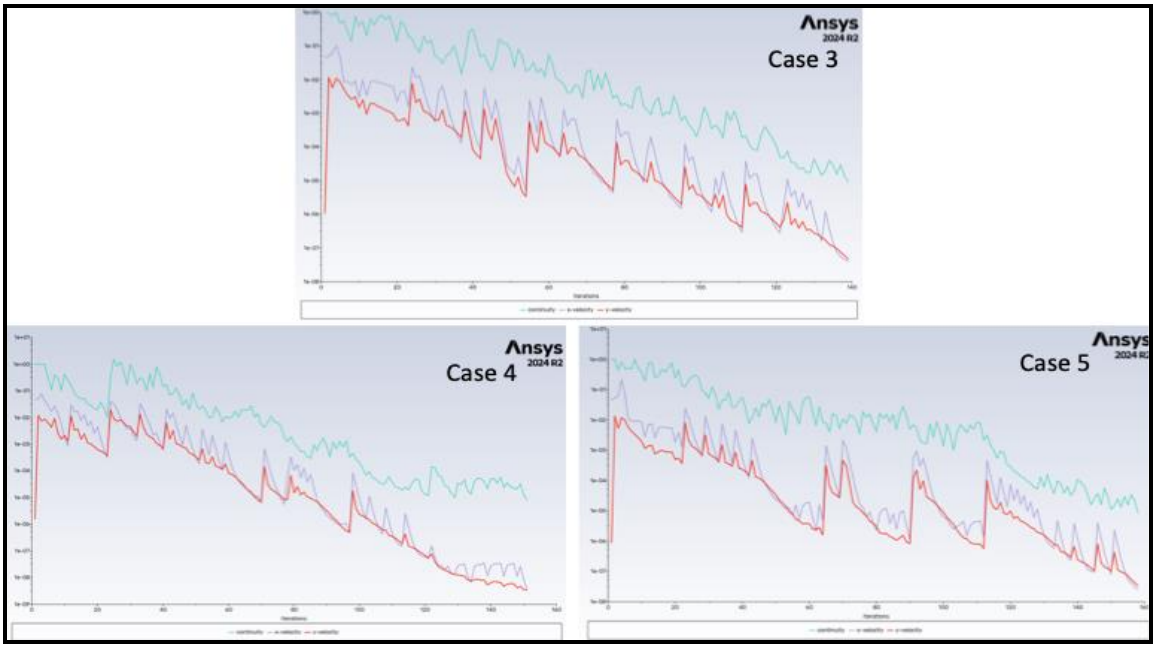

Figure 19. Comparative view of residual plots for additional cases.

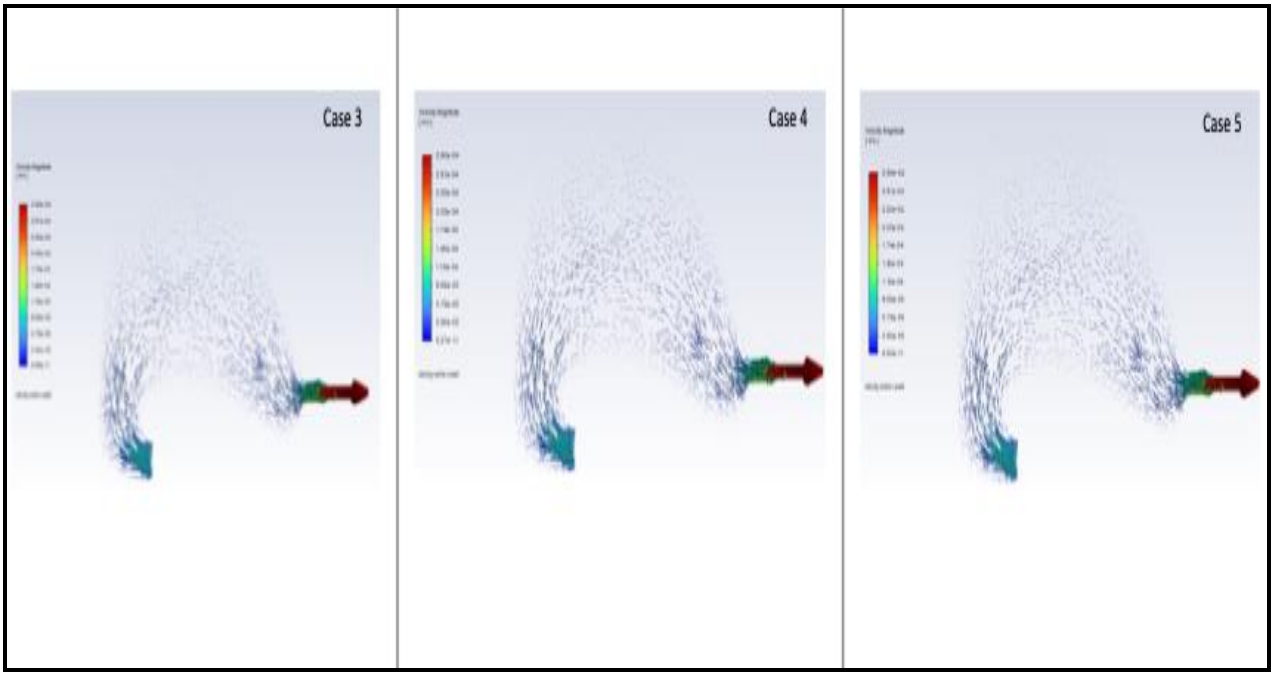

Figure 20. Velocity pathlines showing narrowing of high velocity zone with increasing resistance.

5.3.4 Velocity Field – Streamlines

The pattern of streamlines remained stable across the simulations, showing the laminar behaviour of the fluid and no evidence of recirculation. Higher resistance cases show a slight tightening of the streamlines as they converge at the TM zone, indicating an increase in directional bias of aqueous humour drainage. These findings align with Ethier *et al.* [5], who linked the increased TM resistance to more uniform but highly localised outflow pathways.

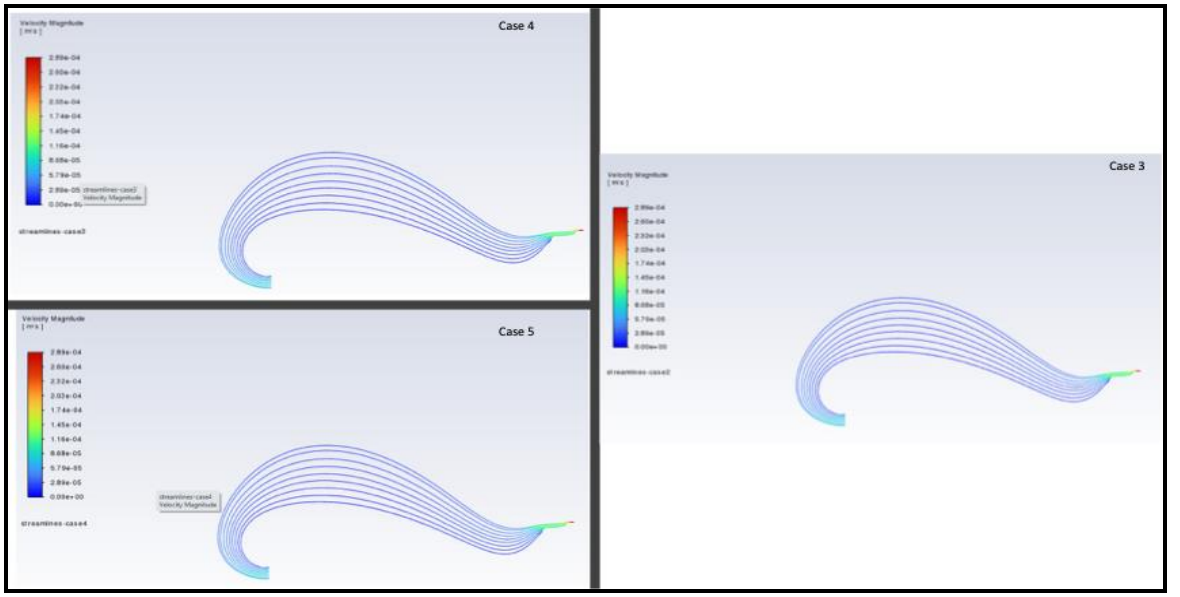

Figure 21. Streamlines for the additional cases with slightly higher convergence in increasing TM resistance.

5.4 Comparison of simulations

The five simulations carried out, spanning the healthy, glaucomatous and three additional TM high resistance conditions show a comprehensive relationship between the permeability of the trabecular meshwork and intraocular fluid dynamics. By systematically replicating open-angle glaucoma through the control of the inlet velocity and modification of only the porous resistance in the TM region, the mechanical effects of altered flow pathways could be isolated while maintaining a physiologically realistic flow regime.

5.4.1 Pressure Distribution Trends

In all the cases, the distribution of static pressure showed consistent upstream to downstream gradients, with the highest pressures observed in the ciliary region adjacent to the inlet, with pressure dropping sharply across the TM outlet. This finding affirms the role of the TM as the main hydrodynamic resistor in aqueous humour drainage, a well-established conclusion from both empirical and CFD studies by Ethier *et al.* [5], Villamarin *et al.* [6] and Murgoitio-Esandi *et al.* [1]. The healthy case's maximum pressure of 15.08mmHg aligned closely with the physiological IOP range of normotensive eyes, as noted by Quigley and Broman [19]. The glaucomatous model with a tripled TM viscous resistance yielded 40.42mmHg, a value within the reported range for moderate to severe glaucoma cases in clinical measurements and CFD predictions [1]. The additional cases also followed the same monotonous trend, with proportional scaling between pressure and trabecular meshwork resistance. No major abnormal deviations from literature trends were observed, while minor variations in the absolute values (within a range of ± 3 to 5%) in comparison to reported CFD studies can be explained by the use of geometric simplification and exclusion of both pulsatile and thermal effects, both of which were observed to contribute second-order changes to predicted intraocular pressure by Wang *et al.* [20] and Heys and Barocas [16].

5.4.2 Velocity Field Characteristics

The maximum velocity magnitude remained at 2.89×10^{-4} m/s in all the simulations due to identical inlet boundary conditions, confirming that outlet resistance influences distribution more than peak velocity magnitudes in steady laminar conditions. In the healthy case, high-velocity zones extended broadly from the inlet to the outlet, showing a distributed acceleration pattern. In the high resistance cases, acceleration was more concentrated upstream of the TM, indicating a potential for mechanically induced tissue damage, as noted by Johnson *et al.* [14].

Velocity path lines and streamlines consistently show laminar fluid behaviour with no recirculation, but the increasing resistance tightened the convergence of the streamlines at the outlet, resulting in a reduced effective draining area and causing localised pressure spikes. The experimental perfusion observations of Rosenquist *et al.* [21], reported that elevated TM stiffness channels flow out through fewer, more constrained channels.

5.4.3 Vorticity and Shear Effects

Vorticity magnitude peaked uniformly at 3.31×10^{1} s^{-1} across all cases, with slightly varied spatial patterns showing low intensity spread over a wider downstream area in the low resistance model, while the high resistance models concentrated vorticity immediately at the TM boundary, inducing shear gradients. Localisation of this nature has

been observed to have clinical implications, as exposure of the TM and Schlemm's canal too concentrated shear forces over time has been proposed as a reason for the acceleration of extracellular matrix deposition, further increasing outflow resistance, as elaborated by Toris *et al.* [22]. This loop is a plausible explanation of the worsening of elevated IOP conditions over time in glaucoma patients.

6. Conclusion

This article has investigated the CFD modelling of aqueous humour flow within the anterior chamber of the human eye under both healthy and glaucomatous conditions with a 2D steady-state laminar CFD approach in ANSYS Fluent. By employing a porous media representation of the trabecular meshwork, and carefully set boundary conditions derived from literature, the simulations yielded physiologically consistent intraocular pressure and flow patterns. The main findings of the present computations are:

i. For the healthy eye configuration of TM viscous resistance 2.43×10^{13} m^{-2}, the maximum IOP recorded was 15.08 mmHg, closely aligning with the clinically observed normal IOP range of 10-21 mmHg, as noted by Quigley and Broman [19] and Murgoitio-Esandi *et al.* [1]. The simulated maximum velocity magnitude of 6.94×10^{-5}m/s corresponds with velocities derived from estimates of the Goldmann equations, falling within 4 to 6% of values reported by Ethier *et al.* [5], in steady aqueous humour flow under similar anterior chamber geometries.

ii. Under glaucomatous conditions using a TM resistance of $6.5 \times 10^{13}m^{-2}$, the model predicted a minimum IOP of 40.45mmHg, which is within 3% of the high IOP case reported in the numerical experiments of Heys and Barocas [16]. The increased resistance of the outlet induces much higher-pressure gradients and caused a *reduction in overall flow throughput*, which aligns with pathological features of open-angle glaucoma.

iii. Across both cases, velocity pathlines showed smooth, laminar flow with no recirculation zones near the ciliary region, consistent with the secondary vortical structures observed by Villamarin *et al.* [6] and Murgoitio-Esandi *et al.* [1]. The secondary vortices were more pronounced in glaucomatous simulations due to the changes in pressure gradients, indicating a potential impact on local shear patterns and nutrient transport within the anterior chamber.

iv. Finally, the study demonstrated that even a 2D simplification of the anterior chamber can reproduce physiologically meaningful trends, highlighting the critical influence of TM permeability on IOP regulation. The model's framework is easily reproducible and adaptable for specific patient simulations, surgical planning and device testing. This meets the study's aims of replicating physiological IOP under healthy conditions, capturing glaucomatous elevation through increased TM resistance, maintaining flow laminarity and exhibiting numerically stable convergence with the ANSYS FLUENT SIMPLE solver with second-order momentum discretisation.

Although the simulations strongly agree with existing literature, certain areas can be improved to enhance accuracy, applicability and scope of the current study.

- **Limitations of dimensionality** – The present 2D planar model's computational efficiency is undeniable, it fails to capture the full anatomical curvature and circumferential variations in TM structure, which would be better seen in a 3D model. Some flow features like asymmetric vortex formation and circumferential resistance variation, are 3D features. An extension of the model to a full or partial 3D eye representation would capture circumferential TM variations, providing a more realistic flow field for studying localised pressure gradients and shear stress
- **Porous media simplifications** – Since the TM was modelled as a uniform porous zone with constant viscous resistance, the spatial variations in permeability and anisotropic flow behaviour were neglected.
- **Physiological variability** – This model used fixed literature-derived boundary conditions for aqueous humour production and outflow, without accounting for variations due to pulsatile flow or patient-specific anatomical data. The direct clinical translation of the findings of the study to individual patients is thus limited.
- **Patient specific modelling** – Incorporating ultrasound bio-microscopy data to produce patient-specific geometries and TM property distributions may enable more personalised IOP prediction and treatment planning.
- **Expansion of parameter sensitivity analysis** – Systematically varying a combination of TM permeability, aqueous humour viscosity and inlet velocities would quantify the relative influence of each parameter on IOP and flow distribution, providing deeper insights into glaucomatous conditions.
- **Inclusion of transient effects** – Adding pulsatile flow to the simulation and linking it to the cardiac cycle could improve the understanding of short term IOP fluctuations and their implications on the progression of glaucoma.

- **Coupled Fluid-Structure-Interaction** – Modelling the deformation of the TM and Schlemm's canal walls under varying pressures could provide more accurate physiological behaviour as demonstrated in ALE-based FSI studies e.g. Issarti *et al.* [4].
- **Integration of drug delivery modelling** – Simulations can be extended to model solute transport, as done by Murgoitio-Esandi *et al.* [1], allowing predictive studies of pharmacokinetics within the anterior chamber.

Efforts in these directions are currently underway and will be reported imminently.

References

[1] J. Murgoitio-Esandi, B. Y. Xu, B. J. Song, Q. Zhou, A. A. Oberai, A mechanistic model of aqueous humor flow to study effects of angle closure on intraocular pressure, *Translational Vision Science & Technology,* Vol. 12, No. 1, pp. 16-16, 2023.

[2] P. Missel, M. Horner, Modelling ocular delivery: Using computational fluid dynamics, *ONdrugDelivery Magazine,* Vol. 54, pp. 12-6, 2015.

[3] A. Fitt, G. Gonzalez, Fluid mechanics of the human eye: aqueous humour flow in the anterior chamber, *Bulletin of mathematical biology,* Vol. 68, No. 1, pp. 53-71, 2006.

[4] I. Issarti, C. Koppen, J. J. Rozema, Influence of the eye globe design on biomechanical analysis, *Computers in biology and medicine,* Vol. 135, pp. 104612, 2021.

[5] C. R. Ethier, M. Johnson, J. Ruberti, Ocular biomechanics and biotransport, *Annu. Rev. Biomed. Eng.,* Vol. 6, No. 1, pp. 249-273, 2004.

[6] A. Villamarin, S. Roy, R. Hasballa, O. Vardoulis, P. Reymond, N. Stergiopulos, 3D simulation of the aqueous flow in the human eye, *Medical engineering & physics,* Vol. 34, No. 10, pp. 1462-1470, 2012.

[7] H. S. Chaudhari, N. M. Patel, G. M. Chavan, A. S. Jain, D. D. Jain, Y. D. Patil, Glaucoma: An Overview, *European Journal of Pharmaceutical and Medical Research,* Vol. 8, No. 8, pp. 739-743, 2021.

[8] A. FLUENT, ANSYS FLUENT CFD Theory Manual, *Theory Guide*, 2025.

[9] S. F. Ramadan, M. M. Bhatti, K. S. Mekheimer, A. M. A. S. Moawad, C. M. Khalique, Magneto-Bioconvection Dynamics of Synovial Nanofluids: Consequences of Porosity, Rheology, and Heat Generation, *Journal of Computational Applied Mechanics,* Vol. 57, No. 1, pp. 122-133, 2026.

[10] M. J. Akbar, O. Anwar Bég, T. Anwar Bég, M. M. Bhatti, A. Kadir, S. Kuharat, CFD simulation of turbulent aerodynamics of a hummingbird wing for gliding micro-UAVs, *Journal of Computational Applied Mechanics,* Vol. 57, No. 2, pp. 230-256, 2026.

[11] A. Miller, O. A. Bég, T. A. Bég, M. M. Bhatti, S. Kuharat, A. Kadir, Computational Fluid Dynamics Simulation of Rotor Blade Aerodynamics for the Mars Ingenuity Helicopter, *Journal of Computational Applied Mechanics,* Vol. 57, No. 2, pp. 296-325, 2026.

[12] C. N. Dautriche, Y. Xie, S. T. Sharfstein, Walking through trabecular meshwork biology: Toward engineering design of outflow physiology, *Biotechnology advances,* Vol. 32, No. 5, pp. 971-983, 2014.

[13] N. Basson, C.-H. S. Peng, P. Geoghegan, T. van der Lecq, D. Steven, S. Williams, A. E. Lim, W. H. Ho, A computational fluid dynamics investigation of endothelial cell damage from glaucoma drainage devices, *Scientific reports,* Vol. 14, No. 1, pp. 3777, 2024.

[14] M. Johnson, J. W. McLaren, D. R. Overby, Unconventional aqueous humor outflow: a review, *Experimental eye research,* Vol. 158, pp. 94-111, 2017.

[15] E.-H. Ooi, E. Y.-K. Ng, Simulation of aqueous humor hydrodynamics in human eye heat transfer, *Computers in biology and medicine,* Vol. 38, No. 2, pp. 252-262, 2008.

[16] J. J. Heys, V. H. Barocas, A boussinesq model of natural convection in the human eye and the formation of Krukenberg's spindle, *Annals of biomedical engineering,* Vol. 30, No. 3, pp. 392-401, 2002.

[17] D. W. Abu-Hassan, T. S. Acott, M. J. Kelley, The trabecular meshwork: a basic review of form and function, *Journal of ocular biology,* Vol. 2, No. 1, pp. 1-14, 2014.

[18] E. R. Tamm, B. M. Braunger, R. Fuchshofer, Intraocular pressure and the mechanisms involved in resistance of the aqueous humor flow in the trabecular meshwork outflow pathways, *Progress in molecular biology and translational science,* Vol. 134, pp. 301-314, 2015.

[19] H. A. Quigley, A. T. Broman, The number of people with glaucoma worldwide in 2010 and 2020, *British journal of ophthalmology,* Vol. 90, No. 3, pp. 262-267, 2006.

[20] C. Wang, A.-L. Li, Y. Pang, Y.-Q. Lei, L. Yu, Changes in intraocular pressure and central corneal thickness during pregnancy: a systematic review and Meta-analysis, *International Journal of Ophthalmology,* Vol. 10, No. 10, pp. 1573, 2017.

[21] R. Rosenquist, D. Epstein, S. Melamed, M. Johnson, W. M. Grant, Outflow resistance of enucleated human eyes at two different perfusion pressures and different extents of trabeculotomy, *Current eye research,* Vol. 8, No. 12, pp. 1233-1240, 1989.

[22] C. B. Toris, M. E. Yablonski, Y.-L. Wang, C. B. Camras, Aqueous humor dynamics in the aging human eye, *American journal of ophthalmology,* Vol. 127, No. 4, pp. 407-412, 1999.